FTMC METINĖS MOKSLINĖS KONFERENCIJOS TEZĖS

2019 m. kovo 6-7 d.
Vilnius

TURINYS

Artūras Plūkis.	Rentgeno ir gama fotonų generavimas didelio galios tankio optine spinduliuote.
Elena Lagzdina.	Branduolinio grafito struktūros pažaidų įtaka radionuklidų pasiskirstymui ir mobilumui matricoje.
Aldona Balčiūnaitė.	Au ir Pt nanodalelėmis modifikuoto Co katalizatorių formavimas apibūdinimas bei taikymas kuro elementuose.
Kastytis Zubovas.	Suardytų žvaigždžių maitinami aktyvūs branduoliai nykštukinėse galaktikose.
Linas Ardaravičius.	Elektronų pernaša ZnO stipriuosiuose elektriniuose laukuose.
Alexandr Belosludtsev.	Investigation of the ultrathin metal films growth and their applications.
Vitalija Rubežienė.	Plataus spektro adaptyvių kamufliažinių medžiagų tyrimai.
Virginija Skurkytė – Papievienė.	Tekstilės medžiagų, dengtų anglies ir bio-PCM dariniais, šiluminės elgsenos tyrimas.
Zigmas Balevičius.	Hibridinių Tamm'o-paviršiaus plazmonų polaritonų modų taikymas gyvsidabrio garų adsorbcijos detekcijai 1D fotoninio kristalo/aukso nanostruktūrose.
Evaldas Naujalis.	Pagrindinės Metrologijos skyriaus cheminių tyrimų kryptys.
Vidmantas Gulbinas.	Naujos fotovoltinių saulės elementų technologijos. Organinių elementų proveržis.
Edvinas Orentas.	Supramolekuliniai nanovamzdeliai: dizainas, sintezė, charakterizavimas ir galimi taikymai.
Mindaugas Gedvilas.	Šiluminė difuzija mikro/nano dariniuose lazerinės interferencinės abliacijos metu naudojant ultra-trumpus impulsus (LMA jaunosios akademijos narys).
Aurimas Vyšniauskas.	Fluorescuojantys klampos sensoriai (apdovanojimas „Metų debiutas“).
Leonas Valkūnas.	Fotoindukuotų vyksmų savireguliacija ir valdymas fotosintezėje (apdovanojimas „Už mokslo pasiekimus“).
Svajus Asadauskas.	Tribocheminių procesų pritaikymas inovatyvių produktų kūrimui (apdovanojimas „Už inovacijas“).

RENTGENO IR GAMA FOTONŲ GENERAVIMAS DIDELIO GALIOS TANKIO OPTINE SPINDULIUOTE

Artūras Plukis, Jonas Reklaitis, Vytenis Barkauskas, Vitalij Kovalevskij, Darius Germanas, Anton Koroliov, Janina Grinevičiūtė, Vidmantas Remeikis

Department of Nuclear Research, Center for Physical Sciences and Technology
arturas.plukis@ftmc.lt

Femtosekundinė lazerio spinduliuotė, sąveikaudama su atomų elektronais, gali indukuoti didelės energijos fotonų emisiją. Rentgeno spinduliuotės trukmė praktiškai lygi pluoštelio trukmei, ir tai leidžia konkuruoti su sinchrotoniniais šaltiniais, kuriems yra būtinas didelės galios greitintuvas. Šiuo metu dažniausiai naudojami mažo atsikartojimo dažnio, didelės galios lazeriai. Tokiu atveju, didinant pluoštelio intensyvumą stebimas Rentgeno spinduliuotės įsisotinimas, kadangi susidariusi plazma ekranuoja gilesnį šviesos įsiskverbimą. Parinkus žadinamo bandinio paviršių ši problema gali būti išvengiama, nes padidėja efektyvus sužadinimas

Tyrimuose panaudojus didelio atsikartojimo dažnio (f=100 kHz) Pharos PH 1-20 lazerio (*Light Conversion*) impulsus (τ=270 fs), naudojant Cu padėklus buvo pasiekta 10^{-7} eilės optinės (λ=1,03 μm) spinduliuotės konversiją į keV eilės energijos nekoherentinę Rentgeno spinduliuotę [1]. Tokių spindulių fotonų energija yra pakankamai didelė, kad būtų galima atlikti tyrimus natūraliomis sąlygomis, ir kartu užtikrinti radiacinę saugą naudojant standartines medžiagas

Tyrimo metu modeliavimo būdu ir eksperimentiškai buvo optimizuojamos lazerinio žadinimo sąlygos, parenkant optimalų taikinio ir lazerinio pluošto parametrų derinį, tirtas femtosekundiniais lazerio impulsais sugeneruotos Rentgeno spinduliuotės pasiskirstymas erdvėje ir tos spinduliuotės išeiga.

Didelės galios, kelių bangos ciklų (τ=15 fs) lazeris (λ=850 nm) su Yb:KGW ir Nd:YAG OPCPA žadinimo sistema panaudotas aukštos energijos (50-80 keV) K-serijos charakteringai spinduliuotei žadinti [2]. Žadinant didelio Z metalus (W, Pt), gauta iki $2{,}5{\cdot}10^{-8}$ eilės spinduliuotės išeiga. Kietoji Rentgeno spinduliuotė gali tapti radiacinės saugos problema netgi už vakuuminės kameros ribų.

Sėkmingai įvykdyti uždaviniai įgalintų verslo partnerius sukurti naujo tipo Rentgeno šaltinio industrinį prototipą

Literatūra

1. A. Baguckis, A. Plukis, J. Reklaitis, V. Remeikis, L. Giniunas, and M. Vengris, Applied Physics B **123**, 290 (2017)
2. J. Reklaitis, V. Barkauskas, A. Plukis, et al. Appl. Phys. B **125**, 41 (2019)

.

BRANDUOLINIO GRAFITO STRUKTŪROS PAŽAIDŲ ĮTAKA RADIONUKLIDŲ PASISKIRSTYMUI IR MOBILUMUI MATRICOJE

Elena Lagzdina, Danielius Lingis, Rita Plukienė, Vitalij Kovalevskij, Artūras Plukis, Vidmantas Remeikis

Department of Nuclear Research, Center for Physical Sciences and Technology
elena.lagzdina@ftmc.lt

Grafitas RBMK, UNGG, Magnox bei HTR tipo reaktoriuose atlieka moderatoriaus bei reflektoriaus funkciją. Grafite esančios priemaišos po 20-30 metų apšvitos yra aktyvuojamos neutronų sraute ir branduolinių reakcijų metu susidaro ilgaamžiai elementai: ^{14}C, ^{36}Cl, transuraniniai elementai. Siekiant teoriškai įvertinti reaktoriaus konstrukcijų aktyvaciją atliekamas kompiuterinis modeliavimas. Didžiausi reaktoriaus modelio neapibrėžtumai kyla ne dėl reaktoriaus darbinių parametrų ir branduolinių duomenų skirtumų, bet dėl priemaišų koncentracijų neapibrėžtumų. GR-280 (kolonos) ir GRP-2-125 (žiedai/įvorės) grafito bandiniai ištirti INAA, PGAA, ICP-MS metodais bei patikslintos priemaišų koncentracijos skirtingose reaktoriaus grafito konstrukcijose (žr. 1 lentelę) [1].

1 lentelė. Vidutinė priemaišų koncentracija RBMK reaktoriaus grafite: kolonoje, žiede bei įvorėje.

	Weighted average of impurity concentrations, ppm			Concentration, ppm	
Element	Stack (GR-280)	Bushing (GRP-2-125)	Sleeve (GRP-2-125)	Maximal limit	Max (Narkūnas et al. 2016)
N			15 ± 4	15	70
Cl	18 ± 4	8.0 ± 0.5	30 ± 1	39	32
Mn	0.16 ± 0.01	0.3 ± 0.02	0.44 ± 0.01	0.64	5
Fe	37 ± 2	22 ± 1	89 ± 3	168	94
Co	(7 ± 2)·10^{-3}	(20 ± 2)·10^{-3}	(29 ± 2)·10^{-3}	0.05	0.063
Ni	0.88 ± 0.09	0.58 ± 0.05	0.63 ± 0.04	1	0.39
Cu	0.57 ± 0.03	0.33 ± 0.02	0.7 ± 0.04	1.4	0.1
Zn	1.4 ± 0.1	1.5 ± 0.1	2.3 ± 0.1	8.1	1.72
Sr	0.16 ± 0.04	0.09 ± 0.01	1.1 ± 0.1	1.1	0.96
Nb			(6 ± 1)·10^{-3}	0.006	
Cs	(3 ± 0.5)·10^{-3}	(2 ± 0.3)·10^{-3}	(2 ± 0.3)·10^{-3}	0.04	0.2
Ba	0.17 ± 0.02	0.14 ± 0.02	1.6 ± 0.1	5.8	2
Eu	(2 ± 0.01)·10^{-3}	(2 ± 0.01)·10^{-3}	(8 ± 0.05)·10^{-3}	0.025	0.3
U	(51 ± 2)·10^{-3}	(13 ± 2)·10^{-3}	(26 ± 3)·10^{-3}	0.066	0.2

Tačiau mikropriemaišų pasiskirstymą grafite nulemia ne tik grafito gamybos procesas (temperatūra, slėgis, žaliavinės medžiagos ir kt.), bet ir grafito eksploatavimo reaktoriuje sąlygos: neutronų srautas, temperatūra, reaktoriaus aplinka (HeN dujų mišinys RBMK atveju). Šie veiksniai apsprendžia radionuklidų pasiskirstymą grafite, o tai svarbu panaudoto grafito radiologiniam charakterizavimui bei tvarkymo technologijos pasirinkimui.

Reaktoriuje greitieji neutronai sąveikauja su grafito konstrukciniais elementais, sukeldami atominio lygio bei mikrostruktūrinius defektus. Šie defektai ilgainiui pakeičia grafito savybes, o taip pat aktyvacijos produktų persiskirstymą grafito matricoje. Teoriškai defektų dinamikos procesai apšvitintame RBMK-1500 grafite įvertinti pasitelkiant kompiuterinį modeliavimą MCNP, GEANT4 bei SRIM-2013 kodais (žr. 1 pav) [2]. Neutronų poveikis RBMK klojinio grafito kristalinei gardelei imituotas atliekant 700 keV 12C+ jonų implantaciją grafito bandiniuose naudojant Tandetron 4110A (*General Ionex Corporation, USA*) jonų greitintuvą [3].

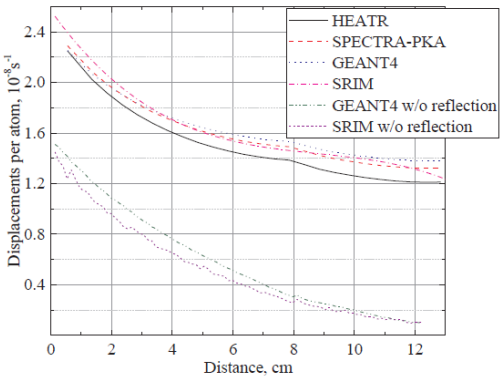

1 pav. Sukuriamų pažaidų (DPA) spartos priklausomybės nuo atstumo grafite naudojant skirtingus modeliavimo kodus.

Atsižvelgiant į RBMK-1500 reaktoriuje palaikomą ~500 ºC temperatūrą, implantuoti bandiniai atkaitinti 400, 600 bei 800 ºC temperatūroje po 5h, tokiu būdu įvertinta grafito struktūros dinamika aukštatemperatūrinėje aplinkoje. Grafito struktūros pokyčiai įvertinti atlikus bandinių paviršiaus Ramano spektroskopinius matavimus.

Literatūra

1. R. Plukienė, E. Lagzdina, L. Juodis, A.Plukis, A. Puzas, R. Gvozdaitė, V. Remeikis, Z. Révay, J. Kučera, D. Ancius, D. Ridikas, Investigation of Impurities of RBMK Graphite by Different Methods, Radiocarbon, (2018) 1-10, https://doi.org/10.1017/RDC.2018.93
2. D. Lingis, E. Lagzdina, A. Plukis, R. Plukienė, V. Remeikis, Evaluation of the primary displacement damage in the neutron irradiated RBMK-1500 graphite, Nuclear Inst. and Methods in Physics Research B 436 (2018) 9-17, https://doi.org/10.1016/j.nimb.2018.08.038
3. E. Lagzdina, D. Lingis, A. Plukis, R. Plukienė, M. Gaspariūnas, I. Matulaitienė, V. Kovalevskij, G. Niaura, V. Remeikis, Structural investigation of RBMK nuclear graphite modified by 12C+ ion implantation and thermal treatment, Nuclear Inst. and Methods in Physics Research B 444 (2019) 23-32, https://doi.org/10.1016/j.nimb.2019.01.049

Au IR Pt NANODALELĖMIS MODIFIKUOTO Co KATALIZATORIŲ FORMAVIMAS, APIBŪDINIMAS BEI TAIKYMAS KURO ELEMENTUOSE

Aldona Balčiūnaitė

Katalizės skyrius, Fizinių ir technologijos mokslų centras
aldona.balciunaite@ftmc.lt

Kuro elementai yra vienas iš atsinaujinančių energijos šaltinių, kuriuose cheminė energija tiesiogiai verčiama į elektros energiją. Jų veikimas pagrįstas kuro oksidacija ant anodo ir deguonies (pastaruoju metu ir vandenilio peroksido) redukcija ant katodo.

Todėl pagrindinis dėmesys skiriamas naujų efektyvių nanostruktūrizuotų medžiagų paieškai, kurios pasižymėtų elektrokataliziniu aktyvumu naudojamo kuro (natrio borohidrido, hidrazino, metanolio, vandenilio ir kt.) oksidacijos ar deguonies (vandenilio peroksido) redukcijos reakcijoms, siekiant padidinti esamų ar naujų kuro elementų našumą.

Šiame darbe Au ir Pt nanodalelės buvo nusodinamos ant kobalto (Co) pluoštine struktūra padengto vario pagrindo. Co pluoštinė struktūra (~3 "m storio) buvo nusodinta taikant elektrocheminį metodą ir suformuojant Co/Cu katalizatorių, o Au ir Pt nanodalelės nusodintos ant pastarojo paviršiaus taikant imersinį metalų nusodinimo metodą.

Au nanodalelės buvo nusodinamos ant Co/Cu paviršių, įmerkiant pastaruosius į 1 mM $HAuCl_4$ + 0,1 M HCl 25 °C temperatūros tirpalą 0,5, 1 ir 5 min. Buvo suformuoti AuCo/Cu katalizatoriai su nusodinto Au įkrova, atitinkamai, 10,9, 22,4 ir 84,4 "g_{Au} cm^{-2}.

Pt nanodalelės buvo nusodinamos ant Co/Cu paviršių, įmerkiant pastaruosius į 1 mM H_2PtCl_6 + 0,1 M HCl 25 °C temperatūros tirpalą 10, 30 ir 60 s. Buvo suformuoti PtCo/Cu katalizatoriai su nusodintos Pt įkrova, atitinkamai, 5,4, 15,4 ir 28,7 "g_{Pt} cm^{-2}.

Suformuotų katalizatorių paviršius buvo detaliai charakterizuojamas skenuojančios elektronų mikroskopijos ir indukuotos plazmos optinės emisijos spektroskopijos metodais, o jų elektrokatalizinis aktyvumas natrio borohidrido ir hidrazino oksidacijai buvo tiriamas, taikant ciklinės voltamperometrijos bei chronoamperometrijos metodus. Gauti AuCo/Cu ir PtCo/Cu katalizatoriai buvo integruojami anodo medžiagomis natrio borohidrido-vandenilio peroksido ($NaBH_4$-H_2O_2) ir hidrazino-vandenilio peroksido (N_2H_4-H_2O_2) kuro elementų prototipuose. Pt elektrodas buvo naudojamas katodu, o anolitu pasirinktas 1 M $NaBH_4$ ar 1 M N_2H_4 šarminis tirpalas, o katolitu - 5 M H_2O_2 + 1,5 M HCl. Kuro elemento matavimai buvo atlikti esant 25, 35, 45 ir 55 ºC temperatūroms.

Panaudojant AuCo/Cu katalizatorių su nusodinto Au įkrova 84,4 μg cm^{-2} kaip anodą, išmatuotas didžiausias galios tankis 25°C temperatūroje yra 188 mW cm^{-2} ir 162 mW cm^{-2}, atitinkamai, $NaBH_4$-H_2O_2 ir N_2H_4-H_2O_2 kuro elementų prototipuose.

Panaudojant PtCo/Cu katalizatorių su nusodinto Pt įkrova 28,7 μg cm^{-2} kaip anodą, išmatuotas didžiausias galios tankis 25°C temperatūroje yra 239 mW cm^{-2} ir 149 mW cm^{-2}, atitinkamai, $NaBH_4$-H_2O_2 ir N_2H_4-H_2O_2 kuro elementų prototipuose.

Remiantis $NaBH_4$-H_2O_2 ir N_2H_4-H_2O_2 kuro elementų prototipų testavimo rezultatais, galime teigti, kad suformuoti AuCo/Cu ir PtCo/Cu katalizatoriai, turintys nedidelius Au ir Pt nanodalelių kiekius, yra perspektyvios medžiagos ir gali būti naudojamos anodo medžiagomis tiesioginiuose natrio borohidrido ir hidrazino kuro elementuose.

ACTIVE NUCLEI POWERED BY TIDALLY-DISRUPTED STARS IN DWARF GALAXIES

Kastytis Zubovas

Department of Fundamental Research, Center for Physical Sciences and Technology
kastytis.zubovas@ftmc.lt

Dwarf galaxies are the smallest dark-matter-dominated stellar systems. They are the building blocks of larger galaxies, and the processes happening within them can help explain many aspects of galaxy evolution.

In recent years, active galactic nuclei (AGN) have been detected in ever more dwarf galaxies, challenging the belief that these objects do not harbour central supermassive black holes (SMBH). SMBH growth and associated feedback via winds is a major driver of galaxy evolution, and so it is natural to ask whether AGN feedback is important in dwarf galaxies. In order to understand this, we need to understand what processes turn on the AGN in dwarf galaxies. It is difficult to feed SMBHs in dwarf galaxies by interstellar gas streams, because star formation is a comparatively more efficient process that consumes gas before it reaches the SMBH. On the other hand, tidal disruption of stars is both more common and more efficient in dwarf galaxies when compared with massive ones, and can be a relevant source of fuel for AGN.

Stars are tidally disrupted when they approach too close to the SMBH. Approximately half the material of the star remains bound to the black hole, forms an accretion disc and feeds the hole, powering an AGN, while the rest of the material is expelled. The rate of tidal disruption events (TDEs) depends on the properties of stellar orbits in the central parts of the galaxy, but in general smaller galaxies have more TDEs per unit time than larger ones. Furthermore, a smaller black hole needs a lower accretion rate to grow significantly, therefore tidal disruptions in smaller galaxies are more important. Combining estimates of TDE rates with estimates of the SMBH mass growth during each event [1], I derive an initial-final mass relationship for SMBHs fed purely by TDEs of Solar type stars for the age of the Universe:

$$M_{\mathrm{f},5} = \left(M_{0.5}^{0.647} + 4.7 \times 10^{-3} \eta_{0.1}^{-0.4} m_*^{0.2} r_*^{0.6} \frac{t}{\mathrm{Gyr}} \right)^{1.546} \quad (1)$$

This equation, as well as the mass change and the total energy release, are plotted as a function of initial mass in Figure 1. We see that very small initial SMBH seeds, with masses of 10^4 Solar masses or less, experience significant growth via tidal disruptions alone.

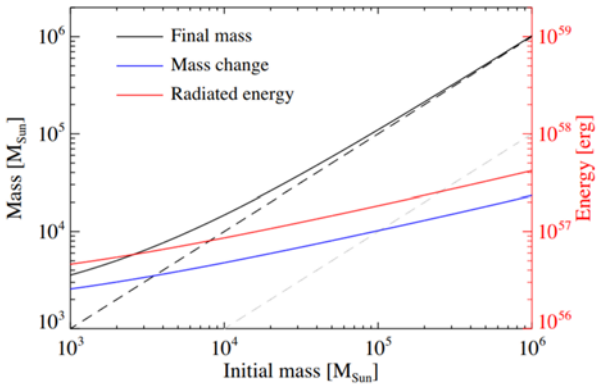

The duration of an AGN episode caused by a TDE also depends on the SMBH mass. In more massive SMBHs, the event lasts only a few years, with luminosity decreasing with time as $t^{-5/3}$ [2]. In smaller galaxies, each flare may last several decades, with a constant luminosity most of the time. This lack of a characteristic luminosity decay, coupled with the long episode duration, may lead to TDEs be misidentified in dwarf galaxies. The fraction of time each dwarf galaxy should have an ongoing TDE-induced AGN episode is consistent with the fraction of dwarf galaxies observed to host AGN [3], assuming that most dwarf galaxies harbour central SMBHs.

Feedback produced by TDE-induced AGN episodes in dwarf galaxies may not be able to drive significant detectable outflows, but it can affect the morphology and orbits of the gas and the stellar population..

Bibliography

1. N.C. Stone and B.D. Metzger, Mon. Not. Roy. Astron. Soc 455, 859 (2016).
2. M. J. Rees, Nature 333, 523 (1988).
3. K. Pardo et al., Astrophys. J. 831, 203 (2016).

HIGH-FIELD ELECTRON TRANSPORT IN ZnO

Linas Ardaravičius[1], Oleg Kiprijanovič[2]

Department of Fundamental Research[1], Department of Material Science and Electrical Engineering[2],
Center for Physical Sciences and Technology
linas.ardaravicius@ftmc.lt

Zinc oxide (ZnO) is a wide bandgap semiconductor, and this material has already found successful applications when a p-n junction is not required in optoelectronic and electronic devices [1]. The transistor high-frequency and high-power performance depends on electron transport at high electric fields. The hot-electron effect is often treated in terms of the dependence of the electron drift velocity on the applied electric field, $v_{dr}(E)$ curve. The expected high theoretic value of the electron drift velocity in wurtzite ZnO at high electric fields (~$3x10^7$ cm/s @ 270kV/cm [2]) promises efficient operation of ZnO-based transistors at centimeter and millimeter-wave frequencies. The simulations clearly demonstrated the negative differential mobility. However, the related experimental studies remain scarce: the ZnO epilayers did not withstand the applied electric field above 150kV/cm at room temperature [3]. The highest value for the electron drift velocity of $1.5x10^7$ cm/s was obtained at the field of 108kV/cm at room temperature for Ga-doped ZnO epilayers with an electron density of $1,4x10^{17}$ cm^{-3}.

This study aims at investigating the hot-electron effects at even higher electric fields: in particular, the velocity-field dependence is measured and calculated for nominally undoped ZnO epilayers at room temperature. The wurtzite ZnO epilayers were grown by plasma-assisted molecular beam epitaxy in Virginia Commonwealth University (USA). The transmission line model patterns (TLM) were processed with evaporated Ti/Au stacks acting as Ohmic contacts. The electron mobility available from the Hall effect measured in the van der Pauw configuration were substantially lower than that obtained from the magneto-resistance measurements carried out on the TLM samples (Table 1), and a new method based on the hot-electron effect was developed in order to estimate the electron drift velocity.

Short voltage pulses were employed in order to minimize the self-heating effects. The field strength of 430 kV/cm is reached with 3 ns pulses without any evidence of the predicted negative differential mobility. Transient measurements have helped to make sure that the electron density is independent of the electric field. The measured current-field dependence is interpreted in terms of the electron drift velocity under the assumption of uniform electric field (Fig.1). The highest electron drift velocity is determined as $2.7\pm0.3x10^7$ cm/s at the electric field of 320 kV/cm [4]. This experimental result approaches the theoretic limit predicted by the known Monte Carlo simulations (solid curve). The Boltzmann kinetic equation is solved within the spherical harmonics expansion (SHE) approach (dashed line) for interpretation of the experimental results; an excellent agreement is obtained.

Table 1. Low-field physical parameters of nominally undoped ZnO epilayers.

Epilayer conductivity σ_0	4,7 S/cm
Electron magnetoresistance mobility	188 $cm^2/(Vs)$
Electron drift mobility μ_0	154 $cm^2/(Vs)$
Electron Hall mobility	53 $cm^2/(Vs)$
Electron density n_0	$1,9x10^{17}$ cm^{-3}

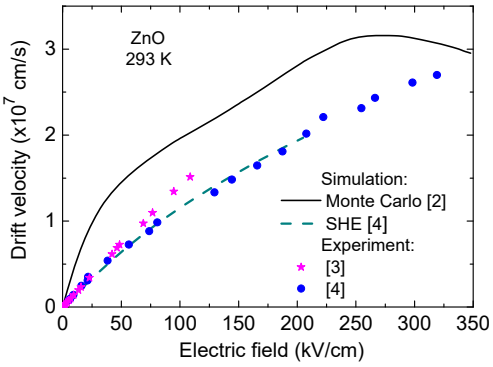

Fig. 1. Drift velocity dependence on the applied electric field at room temperature in ZnO.

This research is funded by the Research Council of Lithuania (grant No. APP-5/2016).

References

1. S. Pearton (ed.), *GaN and ZnO-based Materials and Devices* (Springer, Berlin, 2012).
2. J. D. Albrecht, P. P. Ruden, S. Limpijumnong, W. R. L. Lambrecht, and K. F. Brennan, J. Appl. Phys. **86**, 6864 (1999).
3. L. Ardaravičius, O. Kiprijanovič, J. Liberis, M. Ramonas, E. Šermukšnis, A. Matulionis, M. Toporkov, V. Avrutin, U. Özgur, and H. Morkoç, Mater. Res. Express **4**, 066301 (2017).
4. L. Ardaravičius, O. Kiprijanovič, M. Ramonas, E. Šermukšnis, J. Liberis, A. Šimukovič, A. Matulionis, Md. B. Ullah, K. Ding, V. Avrutin, U. Özgur, and H. Morkoç, [to be submitted].

INVESTIGATION OF THE ULTRATHIN METAL FILMS GROWTH AND THEIR APPLICATIONS

Alexandr Belosludtsev, Naglis Kyžas, Tomas Tolenis,
Audrius Valavičius, Ramutis Drazdys

Department of laser technologies, Center for Physical Sciences and Technology
Alexandr.Belosludtsev@ftmc.lt

Bulk metals are obscure for the light. This is due to free charged carriers in the metals. However, as ultrathin film, metals may behave in a different way. For example, nobel metals structure (Fig.1) and properties non-linearly changes during film growth. This behaivier was investigated real-time in-situ [1]. Three growing stages of metal film on fused silica substrate were in-situ, ex-situ analysed and compared with modelled values.

Detailed analysis of non-continious films was done. For this case, several nanometr thick ultrathin metal films were deposited between alumina layers. In this case, ultrathin film was consist of nanosize particles. Alumina layers were done by atomic layer deposition in order to create the same initial growth conditions for silver and prevent it from possible environment influence. The dependence of particle radius and their distribution, plasmonic peak position on silver thickness and deposition temperature was investigated. One of possible application for ultrathin continious film was show [3]. A novel [4] metal–dielectric three-layer cube broad-angle non-polarizing beam splitter (nPBS) with an ultrathin metal layer was designed, prepared and characterized. Often, nPBS consists of only low and high refractive index layers such as metal oxides, nitrides or fluorides. In some cases, in order to reach the desired specification by formation of dielectic multilayer coatings could be very complicated. In this case, the use of ultrathin metal layer may help, but is requires high precision and process control. Our nPBS structure was prepared in a single process by using of magnetron sputtering. The measured transmittance and reflectance values are in agreement with the design and the desired specification values.

Other possibilty for ultrathin metal application are sensors. It was demonstrated the applicability of multilayered coating with metal film for optical gas sensors technologies [5].

Another structure for tunable sensors was demonstarted. It is possibile to reach of red- and blue-shifts in the spectra by tuning the structure of plasmons based device.

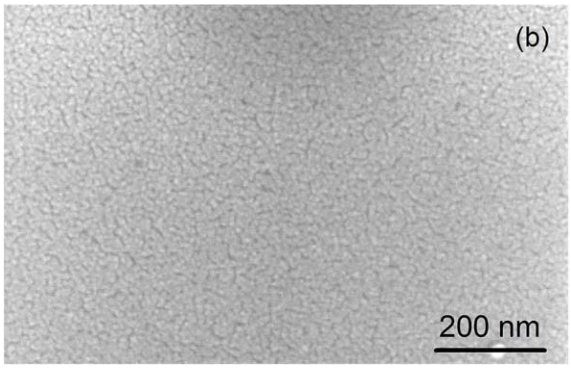

Fig 1. SEM image for 8 nm metal film deposited on fused silica substrate. Here the film growth is in the coalescense stage when isolated metal islands are merging in larger connected structures with nano-holes.

References

1. A. Belosludtsev, N. Kyžas, Mater. Lett. **232**, 216 (2018).
2. A. Valavičius, A. Juršėnas, M. Drazdys, A. Belosludtsev, R. Drazdys, proceedings of OSA Interference coatings conference, submitted (2019).
3. A. Belosludtsev, A. Valavičius, N. Kyžas, S. Kičas, Opt. Laser Technol. **107**, 297 (2018).
4. A. Valavičius, A. Belosludtsev, N. Kyžas, Lithuanian patent application, No. LT2018 505, 09 Feb. 2018.
5. A. Paulauskas, S. Tumenas, A. Selskis, T. Tolenis, A. Valavicius, and Z. Balevicius, Opt. Express **26**, 30400 (2018).

RESEARCH OF WIDE SPECTRUM ADAPTIVE CAMOUFLAGE MATERIALS

Aušra Abraitienė, Vitalija Rubežienė, Diana Kubilienė, Sandra Varnaitė-Žuravliova, Audronė Sankauskaitė

Center for Physical Sciences and Technology
vitalija.rubeziene@ftmc.lt

The key targets of the Long-Term program „Textile technologies and technical fabrics systems" are manly focused on the development of: (i) Smart textile, (ii) functional textile, (iii) theoretical and technological research of clothing protecting against various health and life threats). The investigation and development of military textiles, for today's dismounted soldier systems, is closely related to these targets. One of the main reasons for the fast development of Smart textile is due to its importance given to the military applications. This is because these materials are used in clothing for different atmospheric conditions such as in jackets for extreme winter conditions or in uniforms that should change the colour so as to improve camouflage effects.

Based on previous experience in military camouflage research and recent investigations in the functional textile field FTMC TI in 2018 joined as a partner ~~in~~ the international project „Adaptive Camouflage for the Soldier II (ACAMSII)". This is European Defence Agency (EDA) project, which **received funding from the European Union's Preparatory Action on Defence Research** "PADR-FPSS-01-2017 – Force protection and advanced soldier systems beyond current programmes", **under Grant Agreement No 800871.**

Fig. 1. ACAMSII project logo.

The 3-year project is led by FOI (Sweden). In this project industrial competence, academic and military research institutes, also military end users come together and share their expertise and experiences.

The ambition of the project is to reduce the signature of the soldier and–to increase their survivability and operability (see Fig. 2). The overall concept is to integrate active and passive adaptation mechanisms into the textile-based soldier camouflage system. The system should be capable of sampling and representing the background signature, to adapt to different, changing backgrounds and circumstances (lighting, weather, etc.). The combination of different technologies requires the creation of a multilayer structure in which various devices and materials will be integrated. This is highly essential for strengthening industrial competitiveness and eventually the survivability of the soldier.

Expected impact of the project is dual: strengthening ~~of~~ the competence and thereby the competitiveness of European industry also, in the long run, increased capability of European forces. Adaptive camouflage will give the forces better protection in known environments and the ability to operate in other environments previously considered as too dangerous. Adaptive camouflage will give protection in a variety of military relevant environments against several present and future sensors and sensor systems operating in a wide range of wavelength bands. The project will give an overview of technologies and guidance for promising directions in the future. Also, it will establish methods to address the effectiveness of adaptive and multispectral camouflage against sensors operating in different wavelength regions.

At the end of the project the outcome is expected to give: convincing demonstration of EU-wide research cooperation in defence research; promotion of the integration of interoperability standards; enhanced soldier survivability through protection against a wide range of sensors; enhancement of the effectiveness of military personnel; reduction in life cycle costs; knowledge regarding adaptive camouflage, promising new technologies, requirements, assessment methods and standards.

Fig. 2. ACAMSII overall concept in different environments (conceptual design for adaptive camouflage developed by CITEVE -Technological Textile Center of Portugal).

Acknowledgement
This project has received funding from the European Union's Preparatory Action on Defence Research under Grant Agreement No 800871.

THERMAL BEHAVIOUR OF TEXTILE COATED WITH CARBON AND BIO-PCM DERIVATIVES

Virginija Skurkytė-Papievienė, Aušra Abraitienė, Audronė Sankauskaitė, Vitalija Rubežienė

Department of Textile Technologies and Department of Textiles Physical-Chemical Testing, Center for Physical Sciences and Technology

virginija.skurkyte@ftmc.lt

In this study the thermal behaviour of biological nature phase change material (Bio-PCM) and nano-structures carbon derivatives for textile applications were investigated. As Bio-PCM - butyl stearate (BS) and capric acid (CA) were used and both were encapsulated into the shell of poly-lactic acid (PLA) according to the emulsion/solvent evaporation method [1-2]. The encapsulation effectiveness of PCM, diameter distribution, morphology, latent heat capacity and thermal effectiveness of synthesized PLA/ Bio-PCM microcapsules were determined. The test results have showed the higher encapsulation effectiveness and latent heat capacity of PLA/CA microcapsules. For the improvement of the thermoregulatory properties (thermal conductivity, heat retaining, latent heat capacity) of Bio-PCM micro-capsules the commercial multiwall carbon nanotubes (MWCNT) water dispersion AQUACYL AQ0302 (*Nanocyl SA*) were used. Consequently, 1% and 3% of MWCNT were introduced in to the core and shell of Bio-PCM microcapsules applying two recipes: *a)* MWCNT was dispersed directly in to the PLA/CA dichloromethane solution, *b)* PLA/MWCNT melted composite was dispersed in to the CA dichloromethane solution. Further synthesis of PLA/CA/MWCNT microcapsules was performed according to the same emulsion/ solvent evaporation method. Distribution of microcapsules diameter, encapsulation effectiveness of PCM, latent heat capacity and thermal conductivity of PLA/CA/MWCNT microcapsules prepared by different recipes were determined. The comparative conductivity testing method showed a noticeable increase of thermal conductivity (λ) in PLA/ CA/ MWCNT microcapsules from 0.026 W(m/K) till 0.032 W(m/K) which directly depends from the content of MWCNT in microcapsules. On the contrary, the latent heat capacity (ΔH) was reduced ~10 J/g in comparison with the pristine PLA/CA microcapsules.

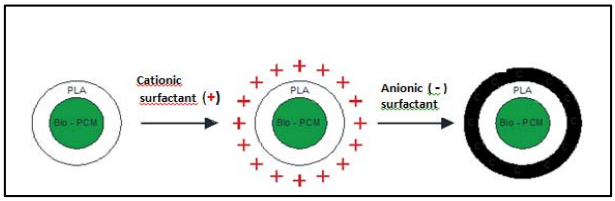

Fig.1. Synthesis of Bio-PCM microcapsules with MWCNT coated PLA shell.

To avoid the leakage of MWCNT to the core and to save the latent heat capacity of Bio-PCM PLA/CA microcapsules with MWCNT coated shell were also prepared (Fig.1). The morphology of these microcapsules was characterized by SEM (Fig. 2, 3). As shown in Fig. 3, on the surface of synthesized PLA/CA/MWCNT microcapsules, MWCNT (length = 1,5 μm, *Nanocyl SA*), are visible.

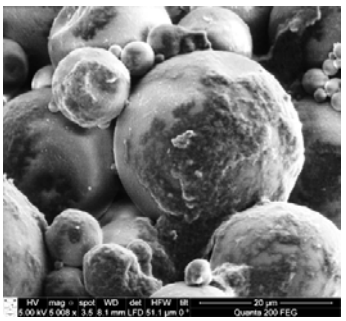

Fig.2. SEM micrograph of synthesized PLA /CA/ microcapsules coated with MCWNT, magnification of 5000.

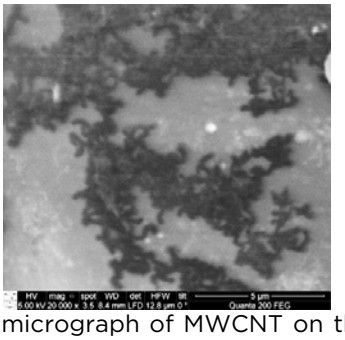

Fig.3. SEM micrograph of MWCNT on the shell of PLA/CA microcapsules, magnification of 20000.

Literature

1. M. Fashandi, S.N. Leung. *Mater Renew Sustain Energy*, (2007, 6:14.
2. M. Fashandi, S.N. Leung. *SPE ANTEC Indianapolis,* 2016, 215-219.

HIBRIDINIŲ TAMM'O-PAVIRŠIAUS PLAZMONŲ POLARITONŲ MODŲ TAIKYMAS GYVSIDABRIO GARŲ ADSORBCIJOS DETEKCIJAI 1D FOTONINIO KRISTALO / AUKSO NANOSTRUKTŪROSE

Zigmas Balevičius, Andrius Paulauskas, Saulius Tumėnas, Algirdas Selskis, Tomas Tolenis, Audrius Valavičius

Department of Material Science and Electrical Engineering, Center for Physical Sciences and Technology
zigmas.balevicius@ftmc.lt

Much attention has been given during the last decade to structures with covered thin metal layers placed on the top of the PC's. Another type of surface mode, the so called Tamm plasmon-polariton (TPP) appears at the boundary between the photonic crystal and the metal layer [1]. Tamm plasmon-polaritons are optical states similar to the electron states proposed by I. Tamm [2], which can occur in the energy band gap on a crystal surface. The stop band of the PC resembles the energy band gap due to Bragg reflections in its periodic structure. In contrast to the SPP propagated surface electromagnetic waves, the TPP are non-propagating states and can be excited in both their TM and TE polarizations (due to the PC) similar to the BSW. The TPPs have an in-plane wave vector, which is less than the wave vector of light in a vacuum, which allows for their direct optical excitation. For the SPPs, this total internal reflection condition can be achieved only when the incident light reaches an in-plane wave vector equal to the surface plasmon resonance. It has been shown [3] that both the TPP and the SPP modes can coexist on the same metal layer if suitable conditions (metal layer thickness and angle of incidence) for both excitations are satisfied and the coupling of these excitations results in the hybrid TPP-SPP mode. For TM polarized incoming light, both the TPP and the SPP are excited at different interfaces of the same metal layer, thus revealing the repulsive nature of these two resonances [3].

Spectroscopic ellipsometry was used for the generation and study of the hybrid TPP-SPP mode as a sensor probe for the real time formation of amalgam structures on the surface of a plasmon active gold layer. The Au/Hg amalgam formation features and the penetration of the mercury atoms into the gold layer were determined by means of the experimental TIRE data and a regression analysis of a multi-layer model containing the index-profile amalgam layer. The hybrid TPP-SPP mode behavior of the coupled excitations gave more information about the penetration of the mercury atoms into the gold layer than the single TPP and SPP resonances. The present study demonstrated the possibility of applying the use of the hybrid TPP-SPP mode for the design of advanced optical gas sensor technologies [4].

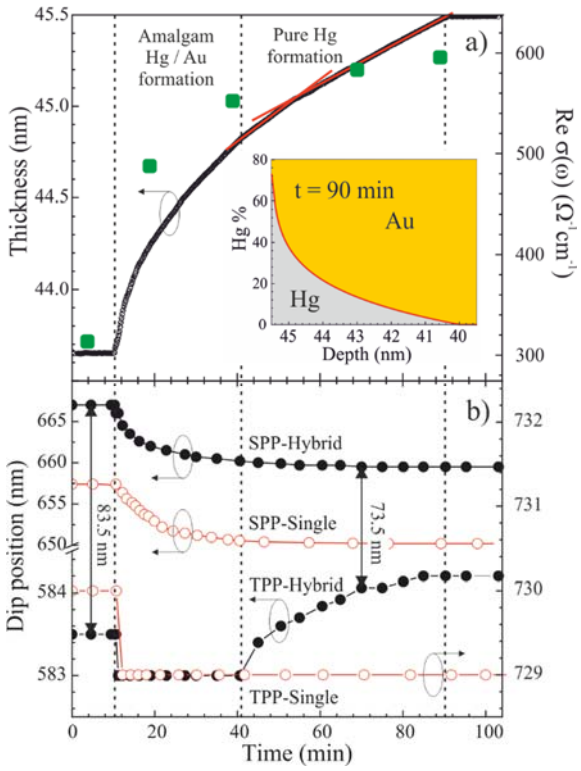

Fig. 1 a) Thickness variation of the amalgam evaluated from regression analysis of the hybrid TPP-SPP mode. The inset shows the depth-profile of the gold and mercury at t = 90 min. Green dots correspond to real part of conductivity of Au/Hg layer at 700 nm wavelength. 5 b) The experimental ( ) dip position dependence on the exposure time of the gold surface in the saturated mercury vapor.

References

1. M. Kaliteevski, I. Iorsh, S. Brand, R. A. Abram, J. M. Chamberlain, A. V. Kavokin, and I. A. Shelykh, Phys. Rev. B **76**, 165415 (2007).
2. I. Tamm, Zeitschrift für Phys. **76**, 849–850 (1932).
3. B. I. Afinogenov, V. O. Bessonov, A. A. Nikulin, and A. A. Fedyanin, Appl. Phys. Lett. **103**, 61112 (2013).
4. A. Paulauskas, S. Tumenas, A. Selskis, T. Tolenis, A. Valavicius, Z. Balevicius, Optics express, **26** (2018) 30400-30408.

MAIN TOPICS OF CHEMISTRY RESEARCH IN METROLOGY DEPARTMENT

Evaldas Naujalis, Birutė Knašienė, Adrian Vicent Claramunt,
Toma Petrulionienė, Audrius Sadaunykas, Audrius Zolumskis

Department of Metrology, Center for Physical Sciences and Technology
evaldas.naujalis@ftmc.lt

FTMC Metrology Department (MD) was authorized to perform and implement functions of the National Metrology Institute (NMI) of Lithuania since 1 July, 2014. It maintains national standards in seven different measurement fields. Laboratory for Metrology in Chemistry (LMiC) is responsible for the metrology in the amount of substance area. The main three directions of activities in LMiC are research in chemical metrology, innovations of measurement instruments and services of chemical analysis for another research institutes, governmental institutions and private companies. Major research areas are: 1) simultaneous elements speciation and isotopic quantification; 2) application of thermal desorption (TD) technique coupled with gas chromatography (GC) for the identification and determination of volatile organic compounds (VOCs); 3) investigation of specific migrants from plastics using chromatography - mass spectrometry; 4) development of accurate and traceable chemical measurement methods for analysis and certification of reference materials; 5) modernization of gas chromatography systems and sampling devices developing new prototypes in order to increase sensitivity and efficiency.

During last year the simple chromatographic method for on-line separation and detection of *3d* transition metal isotopes using ICP-MS have been successfully created [1]. A developed method has been tested in researching the sample of corrosion products from the pipelines of a nuclear power plant (Fig. 1).

Two doctoral dissertation topics are on thermal desorption applications: 1) for research of VOCs in ambient air and human breath to investigate them as potential markers for diagnosis of diseases and 2) for investigation of specific migrants from plastics.

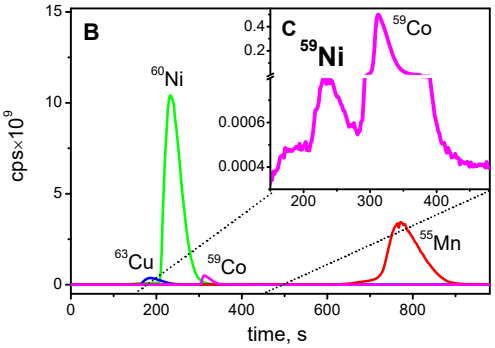

Fig. 1. Chromatograms of ^{55}Mn, ^{59}Co, ^{60}Ni and ^{63}Cu recorded using 0.05 mol/L tartaric acid eluents at pH 4.0 (NH_4OH) and CS5A column. 100 µL injection of: (B) sample of corrosion deposits from the pipelines of NPP; (C) part of the 59 mass chromatogram, in which is visible peak of ^{59}Ni.

Our laboratory is successfully participating in the European Metrology Programme for Innovation and Research (EMPIR) Project ALCOREF 16RPT02 „Certified forensic alcohol reference materials“. The consortium of 10 partners NMIs from 10 different countries was formed with the coordination of Federal Institute for Materials Research and Testing (BAM, Germany). The main activities of the project are research on accurate metrological measurements, homogeneity, short and long term stability estimation for certification of ethanol/water certified reference materials and building of new regional metrological capacity of CRMs production for breath analysers calibration and control.

LMiC provides quantification methods development and chemical analysis services for external customers using chromatography and mass spectrometry. As a good example could be the optimised fast and accurate high liquid chromatography method with spectrophotometric detection for the simultaneous determination of dyes (Solvent Red 19 and Solvent Blue 35) and a marker (Solvent Yellow 124) in diesel fuel [2].

References:

1. D. Plaušinaitis, B. Knašienė, A. Prokopchik, E. Naujalis, A.Vicent Claramunt. Journal of Radioanalytical and Nuclear Chemistry, *DOI:10.1007/s10967-018-5759-7* (2018)
2. A. Markevičius, A. Zolumskis, A. Sadaunykas, B. Knašienė, A. Vicent Claramunt, S. Šakirzanovas, E. Naujalis. Chemija, **29**, No. 2, 121-126 (2018)

NOVEL SOLAR CELL TECHNOLOGIES. BREAKTHROUGH IN ORGANIC SOLAR CELLS

Rokas Jasiūnas[1], Andrius Devižis[1], Feng Gao[2], Vidmantas Gulbinas[1]

[1]Department of Molecular Compounds Physics, Center for Physical Sciences and Technology
[2]Department of Physics, Chemistry and Biology (IFM), Linköping University, Linköping, SE-58183, Sweden
Vidmantas.Gulbinas@ftmc.lt

Electricity generation from solar light energy is rapidly expanding and promises in future to become one of dominating „green“ electricity sources. Si-based solar cells are currently dominating, however more efficient, cheaper, flexible, semi-transparent solar cells are in demand for the wider application of solar cells. A large number of different kinds of solar cell technologies are currently under development. Competition between different technologies is very intense and changeable.

Flexible, solution processed solar cell technologies are very attractive, promising low fabrication price and wide application area. However, such devices based on organic, perovskite, or semiconductor quantum dot materials still show relatively low efficiencies and insufficient lifetime.

Organic solar cells experienced rapid growth in efficiency during the first decade of this century, but later during 5-7 years the achievements were only marginal. Starting from 2017 the organic solar cell efficiency jumped up to more than 17% for tandem architecture [1]. The growth was initiated by application of organic electron accepting materials instead of fullerene derivatives enabling expansion of the cell spectral efficiency to the infrared region.

Despite of these spectacular achievements, many details of the physical processes in all–organic solar cells are still not sufficiently well investigated. Clear understanding is necessary for their further development.

We applied transient spectroscopy technique for investigation of ultrafast photoinduced electronic processes in solar cells with fullerene and two different organic acceptors. Figure 1 shows an example of the investigation results.

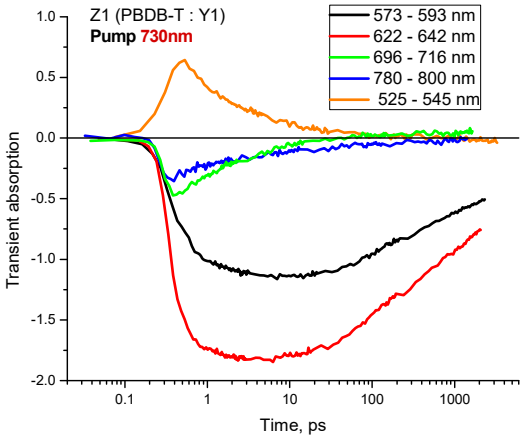

Fig. 1. Transient absorption of PBOB-T (donor)–Y1 (acceptor) solar cell at different probe wavelength under excitation of acceptor material.

The investigations revealed chare separation (initial several picoseconds) and carrier recombination dynamics (hundreds of picoseconds). Comparison of the cell performance shows that cells with organics acceptors experience slightly slower carrier separation and faster carrier recombination in comparison with that with the cell with fullerene acceptor. These are disadvantages of the organic acceptors. Further development of organic acceptors to remove these disadvantages may help to additionally increase the cell efficiency.

References

1. L. Meng et al., Science 361, 1094–1098 (2018).

MODULAR APPROACH TOWARDS TUBULAR MOLECULAR NANO-CONSTRUCTS

Edvinas Orentas, Artūras Ulčinas, Ramūnas Valiokas, Gediminas Niaura, Ieva Matulaitienė

Department of Nanoengineering, Center for Physical Sciences and Technology
edvinas.orentas@ftmc.lt

Tubular molecular structures are among the most versatile constructs that could be assembled in a predictable manner with the help of working principles of supramolecular chemistry. The unique properties of such assemblies are determined by the cylindrical dimensions in which information of directionality is encoded. Nanotubes can perform a variety of functions, such as transport of charged or neutral species, function as template for the synthesis of concave structures or nanowires and provide a nano-space with suitable dimensions for storage or catalytic purposes. We present several unique methods to obtain new types of supramolecular tubular aggregates and polymers, assembled from very small and therefore easily modifiable chiral hydrogen-bonding bicyclic building blocks. The full control of the nanotube structure is possible on the molecular level when careful consideration of tautomeric equilibrium and thus, hydrogen-bonding, is implemented into monomer design. Various aspects of design and characterization of selected hydrogen-bonded tubular aggregates and polymers will be discussed.

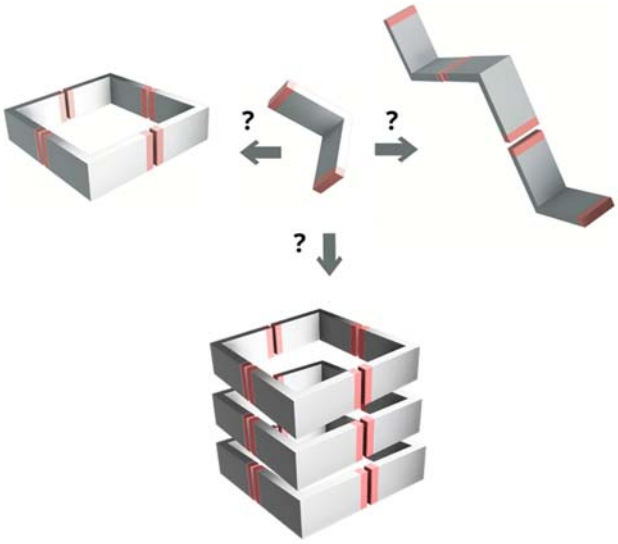

Fig. 1. Selection of various aggregation modes of small complementary molecular building block.

References

1. Q. Shi, T. Javorskis, K.-E. Bergquist, A. Ulčinas, G. Niaura, I. Matulaitienė, E. Orentas and K. Wärnmark, *Nat. Commun*. **8**, 14943 (2017).
2. A. Neniškis, D. Račkauskaitė, Q. Shi, A. J Robertson, A. Marsh, A. Ulčinas, R. Valiokas, S. P Brown, K. Wärnmark and E. Orentas, *Chem. Eur. J*. **24**, 14028 (2018).
3. Q. Chen, X. Su, E. Orentas and Q. Shi, *Org. Chem. Front*. **6**, 611 (2019).

THERMAL DIFFUSION IN MICRO/NANO STRUCTURES FORMED BY LASER INTERFERENCE ABLATION USING ULTRASHORT PULSES

Mindaugas Gedvilas, Simonas Indrišiūnas, Bogdan Voisiat,
Evaldas Stankevičius, Gediminas Račiukaitis
Department of Laser Technologies, Center for Physical Sciences and Technology
mgedvilas@ftmc.lt

Efficient and precise laser texturing of silicon is a critical process in many applications of modern technologies especially for the fabrication of optoelectronic devices and solar cells. The patterning speed over large area can be enhanced by using laser interference ablation (LIA) by ultrashort pulses [1-3]. The highest spatial resolution of the ultrafine LIA is determined by the nanoscale heat transfer during laser-matter interaction time. However, there is no scientific work dedicated to the fundamental law of the laser pulse duration influence on the smallest achievable feature size and highest spatial resolution of LIA. The main purpose of this work is to find the analytical equation binding the interference period and laser pulse duration for ultrafine LIA.

In this research, three-dimensional temperature profiles Fig. 1(a, i) and phase diagrams Fig. 1(a, iii) were computed by finite element analysis solver. The modulation depth of the periodical temperature distribution after LIA was calculated by using $M=(T_{max}-T_{min})/(T_{max}+T_{min})$, where T_{max} - is the temperature in the hottest spatial position at the interference maximum, T_{min} - is the temperature in the coolest spatial position at the interference minimum. The thermal modulation depth dependence on interference period at various pulse durations is given in Fig. 1(b). A new semi-empirical equation binding the pulse duration τ_p, heat diffusion coefficient of material α_{diff}, and thermal modulation depth M for a particular LIA period Λ_4 was introduced in our work [4]:

$$M = (2\Lambda_4 - (\alpha_{diff}\tau_p)^{1/2})/(2\Lambda_4 + (\alpha_{diff}\tau_p)^{1/2}). \quad (1)$$

The Eq. (1) was applied to fit calculated data points in Fig. 1(b). The equation has been verified by experiments and numerical modeling of LIA. Experiments of LIA were conducted by using laser irradiation sources (NL220, Ekspla), (Atlantic HE, Ekspla) and (Pharos, Light Conversion) with pulse durations of 35 ns, 300 ps and 300 fs. Scanning electron microscope (SEM) image of femtosecond LIA in silicon is given in Fig. 1(a, ii). The derived equation is in good agreement with the numerical simulation and experimental results. The new discovered formula can be used for selecting the laser source with required duration of the pulses for periodical interference structuring with required resolution and quality.

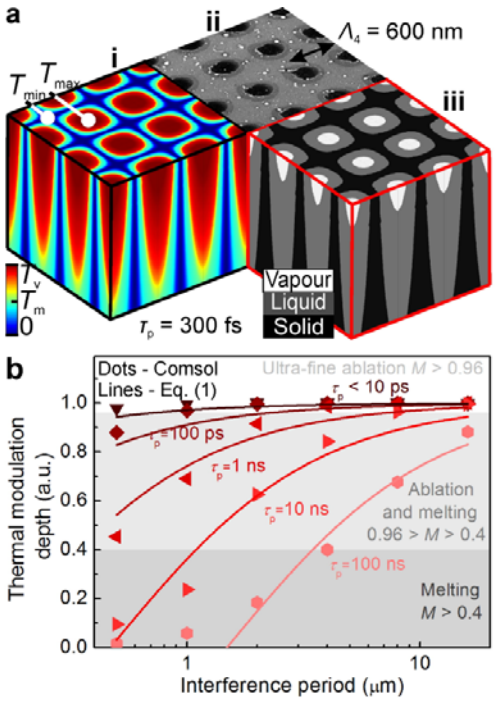

Fig. 1. (a) Computed temperature distribution (i), SEM image (ii) and computed phase diagram (iii) in silicon during LIA: pulse duration τ_p = 300 fs, interference period Λ_4 = 600 nm, laser fluence F_0 = 8.1 J/cm², T_m - melting point, T_v - boiling point, geometry size 1.8 × 1.8 × 1.6 μm³. (b) Thermal modulation depth dependence on interference period at different pulse durations. The regions marked with various grey colors represent the three quality categories of LIA: white - ultra-fine ablation, M > 0.96; light grey - ablation and melting, 0.96 > M > 0.4; dark grey - melting, M < 0.4. Solid dots - Comsol modeling results; solid lines - fit by Eq. (1). Reproduced from ref. [4] with permission from the PCCP Owner Societies.

References

1. M. Gedvilas, B. Voisiat, S. Indrišiūnas, G. Račiukaitis, V. Veiko, R. Zakoldaev, D. Sinev, and E. Shakhno, *Thin Solid Films* **634**, 134 (2017).
2. V. Veiko, M. Yarchuk, R. Zakoldaev, M. Gedvilas, G. Raciukaitis, M. Kuzivanov, and A. Baranov, *Appl. Surf. Sci.* **404**, 63 (2017).
3. S. Indrišiūnas, B. Voisiat, M. Gedvilas, and G. Račiukaitis, *J. Laser Appl.* **29**, 011501 (2017).
4. M. Gedvilas, S. Indrišiūnas, B. Voisiat, E. Stankevičius, A. Selskis, and G. Račiukaitis, *Phys. Chem. Chem. Phys.* **20**, 12166 (2018).

FLUORESCENT VISCOSITY SENSORS

Aurimas Vyšniauskas, Stepas Toliautas, Jelena Dodonova, Sigitas Tumkevičius, Juozas Šulskus, Vidmantas Gulbinas, Marina K. Kuimova

Department of Molecular Compound Physics, Center for Physical Sciences and Technology
aurimas.vysniauskas@ftmc.lt

Fluorescent viscosity sensors – molecular rotors – provide one of the most convenient ways for measuring viscosity in aerosols, model membranes and living cells.[1] However, despite the increasing usage of molecular rotors, the relation between their molecular structure and sensitivity to viscosity or to other parameters, such as temperature and properties of the solvent is not well examined. We have modified the molecular structure of BODIPY-C_{10} (Figure 1A) – one of the most popular molecular rotors – and explored how this impacts the sensitivity of the molecular rotor to viscosity, temperature and solvent properties [2].

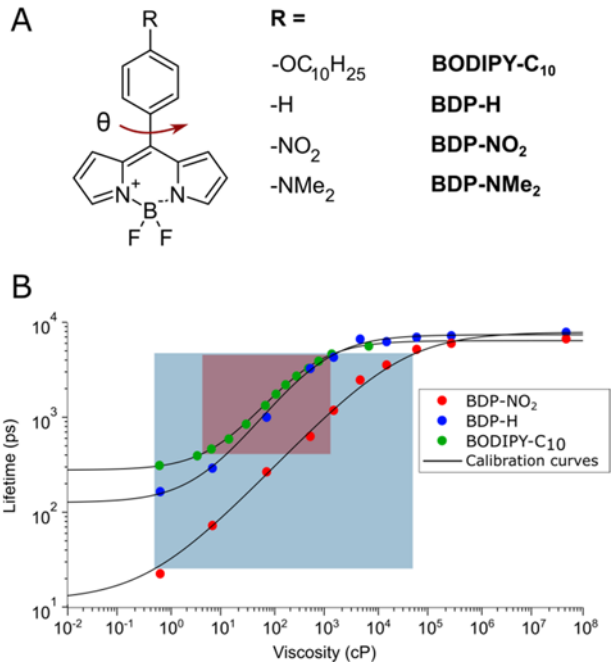

Fig. 1. A) Molecular structures of BODIPY-C_{10} and compounds examined in this work (BDP-H, BDP-NO_2 and BDP-NMe_2. B) Fluorescence lifetime-viscosity dependences of BODIPY compounds. Cherry red and cyan rectangles denote viscosity-sensitive range of BODIPY-C_{10} and BDP-NO_2, respectively.

In this work we varied the substituents on the BODIPY-type molecular rotor, starting with heavy electron-withdrawing –NO_2 group, to electron donating –NMe_2 group (Fig. 1A). Since BODIPY-type rotors are used to sense viscosity via their fluorescence lifetime, we have measured the lifetimes of new BODIPY rotors at varying viscosities, temperatures and in different solvent mixtures.

The rotor with no group (Fig. 1A) possessed very similar viscosity sensitivity properties to BODIPY-C_{10}; its viscosity-sensitive range is approximately 10 cP to 1000 cP, the time-resolved fluorescence decays are shown in Figure 1C. In contrast, the rotor with –NMe_2 group (Figure 1B, right) was non-fluorescent. However, the rotor with –NO_2 was not only fluorescent and viscosity sensitive, but its viscosity sensitive range extended up to 50 000 cP, which makes it much more suitable viscosity probe for high viscosity environments than BODIPY-C_{10}. To our knowledge, this is the first fluorophore capable of viscosity sensing in such viscous environments. Overall, this is an interesting example showing how relatively small changes in molecular structure of molecular rotors can drastically change their properties.

References

1. M. K. Kuimova, Phys. Chem. Chem. Phys., **14**, 12671 (2012).
2. A. Vyšniauskas, I. López-Duarte, N. Duchemin, T.-T. Vu, Y. Wu, E. M. Budynina, Y. A. Volkova, E. Peña Cabrera, D. E. Ramírez-Ornelas and M. K. Kuimova, Phys. Chem. Chem. Phys., **19**, 25252 (2017).

SEF-REGULATION CONTROL ABILITY OF PHOTOINDUCED PROCESSES IN PHOTOSYNTHESIS

Leonas Valkūnas

Department of Molecular Compounds Physics, Center for Physical Sciences and Technology
leonas.valkunas@ftmc.lt

The photosynthetic apparatus of green plants is well-known for its extremely high efficiency that allows them to operate under dim light conditions. On the other hand, intense sunlight may result in over-excitation of the light-harvesting antenna and the formation of reactive compounds capable of "burning out" the whole photosynthetic unit. Non-photochemical quenching (NPQ) is a self-regulatory mechanism utilised by green plants on a molecular level that allows them to safely dissipate the detrimental excess excitation energy as heat. While it is common agreement that the process is place in the plant's major light-harvesting complexes (LHCII), there is still no consensus regarding its molecular nature. To get more insight into its physical origin, high-resolution time-resolved fluorescence measurements of LHCII trimers and their aggregates are analyzed over a wide temperature range [1]. For simulations of the experimental data two-state model as well as multi-state model are formulated and applied. It is demonstrated that both approaches explain the experimental data for the LHCII aggregates resonably well. However, the experiments for the trimers at low temperatures cannot be fitted using the two-state model and can be understood only in terms of the multi-state model [2]. Based on simulations of the excitation energy transfer in the LHCII aggregate, we associate the red-emitting state, having fluorescence maximum at ~700 nm, with the partial mixing of excitonic and chlorophyll–chlorophyll charge transfer states. On the other hand, the quenched state has a totally different nature and is related to the incoherent excitation transfer to the short-lived carotenoid excited states. Our results also show that the required level of photoprotection *in vivo* can be achieved by a very subtle change in the number of LHCIIs switched to the quenched state.

The model developed from the analysis of the fluorescence time-resolved spectral behaviour of LHCII trimers and aggregates has been applied for the description of the fluorescence spectral behaviour of full thylakoid membranes from plants [3]. We demonstrate for the first time that one of the underlying mechanisms is only functional when the reaction center of photosystem II is closed, i.e. when electron transfer is blocked and the risk of photodamage is high. This is accompanied by the appearance of a long-wavelength fluorescence band. As soon as the reaction center reopens, this quenching, together with the long-wavelength fluorescence, disappears instantaneously, what is in line with our previous studies of the fluorescence induction [4]. This allows plants to maintain a high level of photosynthetic efficiency even in dangerous high-light conditions.

These conclusions concerning the relationship between NPQ activity and the state of the reaction center are obtained by taking into account the intrisic mutual dynamic disorder of light-harvesting proteins along with their fluctuating dislocations. On the basis of this presumption a simple conceptual model [5] describing the excitation diffusion in a continuous medium and accounting for possible variations of excitation transfer rates has been developed and applied.

References:

1. J. Chmeliov, A. Gelzinis, E. Songaila, R. Augulis, C. D. P. Duffy, A. P. Ruban, L. Valkunas, Nature Plants, 2: 16045, 2016.
2. A. Gelzinis, J. Chmeliov, A. P. Ruban, L. Valkunas. Photosynth. Res. 135: 275, 2018.
3. S. Farooq, J. Chmeliov, E. Wientjes, R. Koehorst, A. Bader, L. Valkunas, G. Trinkunas, H. van Amerongen, Nature Plants 4: 225, 2018.
4. E. Belgio, E. Kapitonova, J. Chmeliov, C. D. P. Duffy, L. Valkunas, A. P. Ruban, Nature Comm. 5: 5433, 2014.
5. J. Chmeliov, G. Trinkunas, H. van Amerongen, L. Valkunas, J. Am. Chem. Soc., 136: 8963, 2014.

UTILIZATION OF TRIBOCHEMICAL PROCESSES FOR DEVELOPMENT OF INNOVATIVE PRODUCTS

Svajus Asadauskas

Department of Electrochemical Material Science, Center for Physical Sciences and Technology
svajus.asadauskas@ftmc.lt

During the interactions between moving surfaces a variety of chemical reactions take place. Thermochemical processes predominate, but catalytical, oxidative and even plasma reactions are commonplace in a friction zone. In contrast to mechanochemical processes, which can proceed deep inside the material without any involvement of friction, tribochemical reactions affect only the top layers, usually within less than 1 ″m from the surface. However, in liquid, highly porous or elastic materials, friction-induced processes can be significant in deeper layers as well [1]. This creates favorable conditions to develop new materials using tribochemical interactions.
Accurate control of tribological parameters is very important when investigating the extent of friction-induced effects. A specialized tribotest, based on thin oil film, was set up to study the transformations in oil caused by friction.

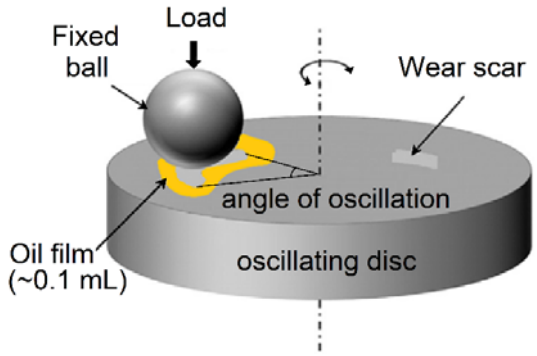

Fig. 1. Schematic setup of ball-on-disc oscillatory tribotest. Not to scale.

Tribometer MicroPoD TR-20 M63 (Ducom Instruments Pvt Ltd.) was used with a fixed 6 mm OD ball of steel 100Cr6, grade G100, roughness Ra 0.10 ″m (RGP International Srl). Oil film of total 0.1±0.05 mL sample volume was applied onto the area around the ball making sure that oil starvation would not take place. Oscillatory (reciprocal) rotational trajectory produced a wear scar of 5.2 mm length, while 1 Hz oscillation led to 1 cm/s tangential velocity. Load was applied pneumatically at 50 N or higher values. Friction results in wear scars on the disc and the ball. Their depth depends not only on the load and velocity of moving surfaces, but also on their hardness.
Size of wear scars relates to friction intensity, but variation in hardness might make such correlation problematic. Therefore, the steel ball was inspected for homogeneity of its hardness. In addition, distribution of Cr %wt. in deeper layers was also evaluated, since this element is often used to produce hard alloys.

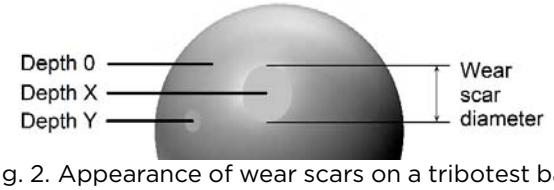

Fig. 2. Appearance of wear scars on a tribotest ball. Not to scale.

Vickers microhardness (HV) under 50 g load [2] procedure and EDX spectroscopy were used for the analyses respectively. Fig. 3 demonstrates their results from wear scars, produced by abrasive material.

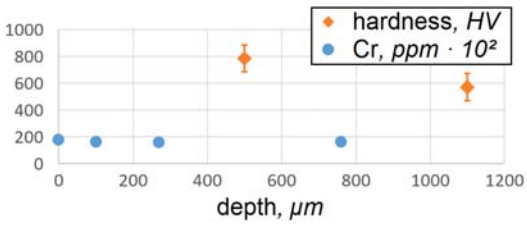

Fig. 3. Changes in Vickers microhardness (HV) in deeper layers of the test ball with Cr contents (mass-to-mass) for comparison.

Although hardness variation is not negligible, statistically it is not possible to provide a quantifiable gradient. It might be suspected that steel is softer in deeper layers. Nevertheless, the variation is small and measurements of wear scar diameter provide a relatively proportional assessment of wear intensity.

Acknowledgment
Tadas Matijošius, Gedvidas Bikulčius and Giedrius Stalnionis performed the measurements. Ignas Valsiūnas and Antanas Strakšys (all FTMC) suggested the need for this study.

Literature

1. S. J. Asadauskas, A. Jukna *Devulcanizing agent for production of reclaim rubber powder*, European patent EP 2 909 240 B1, 2014, pp 1-22. Also adapted and registered as WO 2014062043 A1; CN 104334585 A; RU 2611492 C2; IN02292MUN2014A and US 2015/0197581 A1.
2. T. Matijošius, A. Kalužina, G. Bikulčius, I. Valsiūnas, S. Asadauskas, *Comparison of liquid friction trend between steel and several bioceramic surfaces,* FizTeCh doktorantų ir jaunųjų mokslininkų konferencija, NFTMC Vilnius, October 18, 2018, p 44.